the most important effect. These processes are found in all nuclei in which a high j-shell exists in the vicinity of the Fermi surface. However, it is another question as to whether they produce backbending. This depends finally on the strength of the interaction between the two crossing bands: Only for rather small coupling matrix elements do we observe a sudden transition, that is backbending.*

3.3.3 The Triaxial Particle-plus-Rotor Model

We have already seen in Section 1.5.3 that Davydov et. al. [DF 58] used a triaxial rotor to explain the low lying 2^+ states in some transitional nuclei. The model can also be extended to odd mass nuclei by the coupling of an external particle to a triaxial rotor [Pa 61, HS 62, PR 62, PS 65, MSD 74, Me 75, FT 75, TF 75, Le 76, DF 77, LLR 78]. It has been applied to cases where the external particle sits in a high j-shell, and has turned out to be very powerful as a description of energy levels and decay schemes of many transitional nuclei.† However, at present the microscopic foundation is missing. Using microscopic theories, the calculations of static energy surfaces in these mass regions show no pronounced minima at triaxial deformations, which would justify this simple picture. In fact, there exist other models based on a *vibrational picture* [AP 76, PVD 77, YNN 76] that are also able to reproduce such spectra. It is not clear at present whether there is any connection between these two pictures of transitional nuclei.

We restrict ourselves in the following discussion to one external particle in a high j-shell (e.g., h 11/2) and couple it to a triaxial rotor. In this case, the Hamiltonian has the form [MSD 74]:

$$h = \sum_{i=1}^{3} \frac{R_i^2}{2\mathcal{I}_i} + h_0 + kr^2\beta \left\{ \cos\gamma\, Y_{20} + \sin\gamma \frac{1}{\sqrt{2}} (Y_{22} + Y_{2-2}) \right\}. \tag{3.59}$$

The β, γ-dependence of the moment of inertia $\mathcal{I}_i$ is that for irrotational flow [eq. (1.48)] and only the overall constant is adjusted. The constant k is given by the splitting of the j-shell in the Nilsson scheme. h_0 is the spherical harmonic oscillator. Usually a single-particle pairing field with constant gap Δ is also taken into account.

Figure 3.12 shows the spectrum of the Hamiltonian (3.59) as a function of γ at a typical deformation $\beta = 5A^{-2/3}$. On the prolate side ($\gamma = 0$) and on the oblate side ($\gamma = 60°$) we see again the same spectra as in Fig. 3.10. However, these two limits are now connected through a circle in the β, γ plane (Fig. 1.4) with constant deformation β. We no longer pass through the weak coupling limit at $\beta = 0$. On both sides the spectra do not depend very drastically on the triaxiality γ. The essential transition from the strongly coupled to the decoupled scheme takes place in a relatively small γ region around $\gamma = 30°$. There are many spectra in weakly deformed transitional nuclei that can be nicely reproduced with γ-values between 20° and 40°. This agreement can be improved even more by incorporating the change of the moment of inertia in a VMI-model type calculation [FT 75].

* Recently, Bengtsson et al. [BHM 78] have found an oscillating behavior of this interaction as a function of the chemical potential λ. For an interpretation of this fact see [FPS 80] and the references given there.

† For extension of the triaxial rotor model to multiparticle configurations, see [TNV 77, YTF 77, TYF 77, YTF 78].

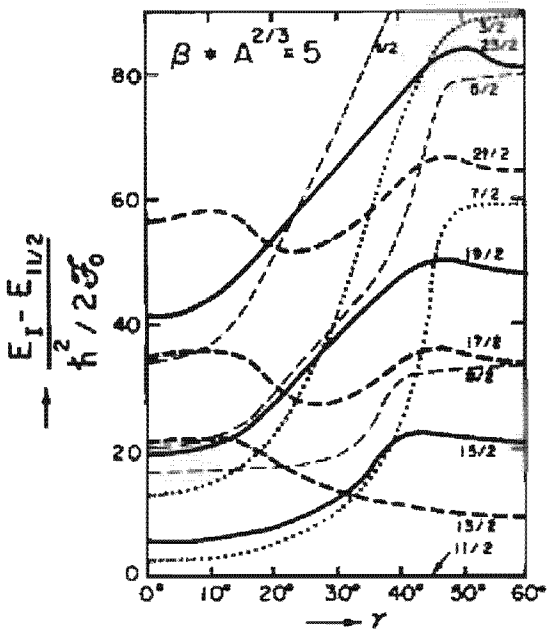

Figure 3.12. Spectrum of a $j = 11/2$ particle coupled to an asymmetric rotor with all yrast levels $I < 23/2$ as function of γ. (From [MSD 74].)

The *dynamical behavior* of a system of an odd high-j particle coupled to a rotating triaxial core is determined by three physical effects (see [Me 75]):

(i) The core prefers to rotate around the axis with the maximal moment of inertia in order to minimize the rotational energy.
(ii) The particle moving in the deformed well prefers maximal mass overlap with the core, because in this case its potential energy is minimal.
(iii) The Coriolis interaction tries to align the angular momenta of the particle **j** and the core **R**.

For high j-values the alignment dominates as long as we have only one particle in the j-shell. Since the density distribution of an aligned particle is oblate with j as symmetry axis, condition (ii) is optimally satisfied if the core is oblate ($\gamma = 60°$), which corresponds to the 2-axis as the symmetry axis. However, in this case $\mathfrak{I}_2 = 0$ and condition (i) is violated. Therefore, **R** will be perpendicular to the 2-axis and we no longer have alignment. In the triaxial case, $\mathfrak{I}_2$ no longer vanishes and conditions (i), (ii), and (iii) can all be satisfied together. There is an alignment of **j** and **I** along the 2-axis. In fact, the calculations show that the odd particle tends to align along the 2-axis of the core. This axis serves as an approximate symmetry axis in the sense that the approximate quantum numbers $\bar{K}$ and $\bar{\Omega}$ (representing the projections of **I** and **j** onto the 2-axis) are meaningful for a classification. The result is a new level scheme characteristic for a triaxial rotor.

The yrast levels are given by $\bar{\Omega} = j$ and $\bar{K} = j, j \pm 2, j \pm 4$, as in the rotation aligned coupling scheme of Stephens. For these levels, **I**, **j**, **R**, and the 2-axis are parallel. They lie on the usual parabola with $\Delta I = 2$ (see Fig. 3.13). Contrary to the axial symmetric case, where the direction of the alignment was arbitrary in the 1, 2 plane (usually one chooses the 1-axis), we have the asymmetric case with no such symmetry. Alignment favors the 2-axis. This has the consequence that on each yrast level there exists a rotational band with the spin order $\Delta I = 1$. In fact, such levels have been experimentally observed [ABR 75].

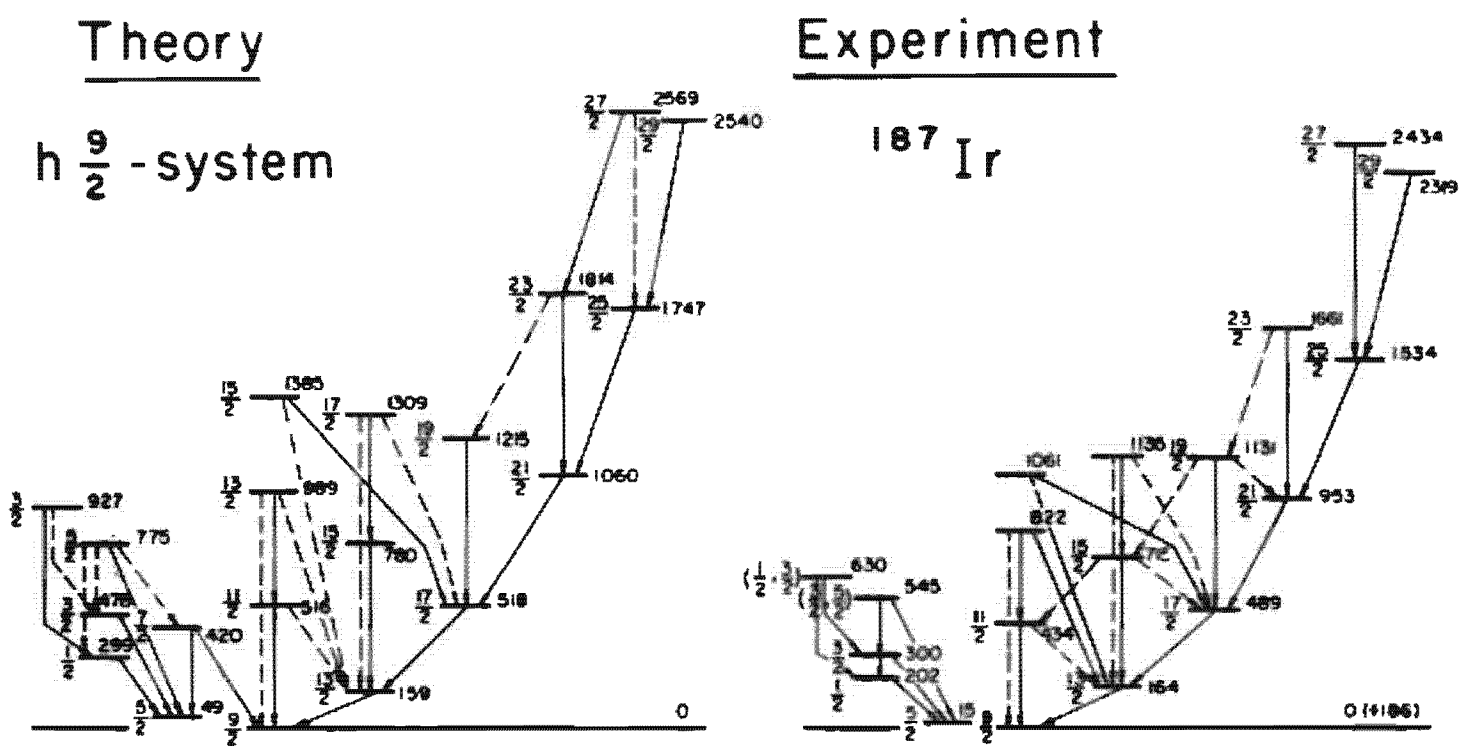

Figure 3.13. The $h_{9/2}$ family of negative parity states in ^{187}Ir. (From [Me 75].)

3.3.4 Electromagnetic Properties

According to the separation of the system into valence particles and a core, we also have two contributions for the electromagnetic multipole operators:

$$Q_{\lambda\mu} = Q^{(c)}_{\lambda\mu} + Q^{(p)}_{\lambda\mu}. \tag{3.60}$$

The core part is given by Eq. (1.35) and $Q^{(p)}$ is defined in Eqs. (B.23, B.24) where the sum over i however is restricted to the number of valence particles.

In the following we shall restrict ourselves to the axially symmetric case without pairing. It is then relatively simple to generalize the formulae to more complicated cases.

The *magnetic dipole moment* of the rotor is given by Eq. (1.36) as $\mu = \mu_N \cdot g_R \mathbf{R}$. We therefore gain for the $M1$ operator:

$$\mathrm{M}_1 = \sqrt{\frac{3}{4\pi}}\ \mu_N \cdot g_R (\mathbf{I} - \mathbf{J}) + \mathrm{M}_1^{(p)}. \tag{3.61}$$

The magnetic dipole moment is defined in Eq. (B.31). With the wave function of Eq. (3.25) we obtain for $K \neq 1/2$, using the projection theorem (2.66),

$$\mu = \sqrt{\frac{4\pi}{3}}\ \langle \Psi^I_{IK} | M_{1z} | \Psi^I_{IK} \rangle = \mu_N \left\{ g_R \frac{I(I+1) - K^2}{I+1} + g_K \frac{K^2}{I+1} \right\} \tag{3.62}$$

where we have introduced the gryomagnetic ratio g_K in the following way.

$$\begin{aligned} g_K \cdot K &= \frac{1}{\mu_N} \sqrt{\frac{4\pi}{3}}\ \langle \Phi_K | M^{(p)}_{13} | \Phi_K \rangle \\ &= \langle \Phi_K | g_s \cdot s_3 + g_l l_3 | \Phi_K \rangle \\ &= g_l K \cdot + (g_s - g_l) \cdot \langle \Phi_K | s_3 | \Phi_K \rangle. \end{aligned} \tag{3.63}$$

The matrix element $\langle \Phi_K | s_3 | \Phi_K \rangle$ can be calculated with a Nilsson wave function. For $K = 1/2$ one gets an additional contribution to the magnetic moment which contains the decoupling factor a of Eq. (3.30).

The magnetic moments obtained from Eq. (3.62) have been calculated for a large range of nuclei [MN 59, NN 65 p. 653] and one has found that agreement with experimental data is usually better for protons than for neutrons. A detailed investgation shows, however, that one again needs polarization charges for g_s: $g_s^{\mathrm{eff}} \simeq 0.7 g_s^{\mathrm{free}}$ (see [BM 75 p. 302ff]).

Similarly, we can calculate the reduced matrix elements for $M1$-*transitions*. The operator I does not cause any transitions. For the rest we use Eq. (1.70) and get for $K \neq 1/2$ and $I_i \neq I_f$:

$$B(M1, I_i \to I_f) = \frac{1}{2I_i + 1} \left| \langle \Psi^{I_f}_K \| M_1 \| \Psi^{I_i}_K \rangle \right|^2 = \frac{3}{4\pi} \mu_N^2 (g_K - g_R)^2 K^2 \left| C^{I_i\ 1\ I_f}_{K\ 0\ K} \right|^2. \tag{3.64}$$

These $M1$-transitions are only possible for rotational bands in odd nuclei. Also, reasonable agreement with experiment has been found [SBP 67].

Again using Eq. (1.70) we can also derive the $B(E2)$ values for *electric quadrupole transitions*. For transitions between states with the same K value the core contribution is much larger than the particle contribution because of the large Q_0 values. Therefore, the latter can be neglected, and we obtain

$$B(E2, I_i \to I_f) = Q_0^2 \frac{5}{16\pi} \left| C^{I_i\ 2\ I_f}_{K\ 0\ K} \right|^2. \tag{3.65}$$

This equation is used to determine the experimental values for the deformations appearing in Q_0. In Sec. 2.8.6 we saw that they agree with the theoretically determined deformations. Therefore, the particle-plus-rotor model gives the proper $E2$ transition probabilities for transitions with the same K-value.

For transitions with different K-values, the collective part vanishes. Such transitions are, in fact, very weak (*K-forbidden*) because the single-particle part contains only the single-particle matrix element of r^2Y_{20} in the intrinsic frame. We have already seen in Section 2.7.2 that they are small compared to the collective values. On the other hand, a pure single-particle model cannot explain the effective charges in spherical nuclei (see Sec. 2.7.2). The same difficulties occur here again. For a detailed discussion, see the paper of Löbner and Malinskog [LM 66], which contains much experimental data together with possible ways to improve the simple Nilsson estimate.

Finally, we have to mention that the above considerations apply only to pure K-bands. For transition probabilities and electromagnetic moments in K-mixed bands, like rotational aligned bands or bands in an asymmetric rotor, we have to take into account the mixing coefficients.

3.4 The Cranking Model*

We have seen in the last section how the motion of particles in a deformed well can be connected with the idea of a rigid rotor. This model is very successful in the description of the level structure of rotational and even transitional nuclei. However there exists no straightforward microscopic derivation; in particular, one cannot calculate the inertial parameters in this model.

On the other hand, nearly all fully microscopic theories of nuclear rotation are based on or related in some way to the cranking model, which was introduced by Inglis [In 54, 56] in a semiclassical way, but as we shall see in Section 11.4, it can be derived fully quantum mechanically, at least in the limit of large deformations, and not too strong K-admixtures ($K \ll I$).

The cranking model has the following advantages.

(i) In principle, it provides a fully microscopic description of the rotating nucleus. There is no introduction of redundant variables, therefore, we are able to calculate the rotational inertial parameters microscopically within this model and get a deeper insight into the *dynamics* of rotational motion.

(ii) It describes the collective angular momentum as a sum of single-particle angular momenta. Therefore, collective rotation as well as single-particle rotation, and all transitions in between such as decoupling processes, are handled on the same footing.

(iii) It is correct for very large angular momenta, where classical arguments apply (even if the quantum mechanical derivation does not work in this limit [BMR 70]).

* In this chapter, we treat only cranking theory for rotations. We can, however, also apply a similar theory for general collective motions, as discussed in Section 12.3.7.